NASA TECHNICAL NOTE

NASA TN D-4766

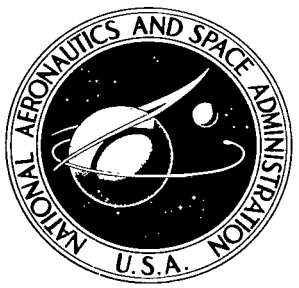

A COMPUTER PROGRAM FOR SYSTEMATICALLY ANALYZING FREE-FLIGHT DATA TO DETERMINE THE AERODYNAMICS OF AXISYMMETRIC BODIES

by Gerald N. Malcolm and Gary T. Chapman

Ames Research Center
Moffett Field, Calif.

NATIONAL AERONAUTICS AND SPACE ADMINISTRATION • WASHINGTON, D. C. • SEPTEMBER 1968

A COMPUTER PROGRAM FOR SYSTEMATICALLY ANALYZING FREE-FLIGHT DATA TO DETERMINE THE AERODYNAMICS OF AXISYMMETRIC BODIES

By Gerald N. Malcolm and Gary T. Chapman

Ames Research Center
Moffett Field, Calif.

NATIONAL AERONAUTICS AND SPACE ADMINISTRATION

For sale by the Clearinghouse for Federal Scientific and Technical Information
Springfield, Virginia 22151 – CFSTI price $3.00

A COMPUTER PROGRAM FOR SYSTEMATICALLY ANALYZING FREE-FLIGHT DATA TO DETERMINE THE AERODYNAMICS OF AXISYMMETRIC BODIES

By Gerald N. Malcolm and Gary T. Chapman

Ames Research Center

SUMMARY

The computer program analyzes free-flight motions of axisymmetric bodies to deduce coefficients of drag, lift, and static and dynamic stability from any set of free-flight data complete enough to define the trajectory and angle history. Nonlinear behavior can be accurately assessed from the results of the data-reduction program, and available methods are discussed. To demonstrate the effectiveness of the data-reduction method, free-flight tests of the AGARD standard hypersonic ballistic correlation model HB-2 were conducted. The results for lift and static and dynamic stability at a Mach number of 2 agreed well with conventional wind-tunnel results. Significant differences were found in the drag data because of different base pressures believed due to sting effects in the wind-tunnel tests.

INTRODUCTION

Free-flight techniques have been used at Ames Research Center, in both ballistic ranges and counterflow facilities, to obtain aerodynamic characteristics of many types of configurations. In past years, raw data were reduced principally for drag and stability and only occasionally for lift. The procedures involved several computer programs and a substantial amount of manual calculation.

Recently, a Fortran IV computer program was developed to systematize the data-reduction procedure and eliminate all manual calculations. The program produces in one operation a set of quasi-linear values[1] for the aerodynamic coefficients of drag, lift, and static and dynamic stability. Improved procedures have been incorporated to calculate drag coefficients, and the method of determining lift and stability coefficients has been modified to reduce errors.

To demonstrate the effectiveness of the data-reduction method, it is applied to free-flight data from tests of the AGARD standard hypersonic

[1]The values are termed "quasi-linear" since the equations of motion that are solved explicitly assume the static forces and moments are either constant or vary linearly with angle of attack and dynamic forces and moments vary linearly with angular rate.

ballistic correlation model HB-2, and the results are compared with conventional wind-tunnel results (refs. 1-3).

SYMBOLS

A	reference area, $\frac{\pi d^2}{4}$
C_D	drag coefficient, $\frac{\text{drag}}{q_\infty A}$
C_L	lift coefficient, $\frac{\text{lift}}{q_\infty A}$
C_{L_α}	lift-curve slope, $\frac{\partial C_L}{\partial \alpha}$
C_{L_o}, C_{y_o}	trim lift and side-force coefficients at $x = 0$
$C_{L_{p\alpha}}$	Magnus force, $\frac{\partial^2 C_L}{\partial \left(\frac{pd}{V}\right) \partial \alpha}$
$C_{L_q} + C_{L_{\dot\alpha}}$	lift due to pitching and plunging, $\frac{\partial C_L}{\partial \left(\frac{qd}{V}\right)} + \frac{\partial C_L}{\partial \left(\frac{\dot\alpha d}{V}\right)}$
C_m	pitching-moment coefficient, $\frac{\text{pitching moment}}{q_\infty A d}$
$C_{m_{\alpha_l}}$	quasi-linear value of pitching-moment-curve slope
$C_{m_{p\alpha}}$	Magnus moment (static), $\frac{\partial^2 C_m}{\partial \left(\frac{pd}{V}\right) \partial \alpha}$
$C_{m_{pq}} + C_{m_{p\dot\alpha}}$	Magnus moment (dynamic), $\frac{\partial^2 C_m}{\partial \left(\frac{pd}{V}\right) \partial \left(\frac{qd}{V}\right)} + \frac{\partial^2 C_m}{\partial \left(\frac{pd}{V}\right) \partial \left(\frac{\dot\alpha d}{V}\right)}$
$C_{m_q} + C_{m_{\dot\alpha}}$	damping-in-pitch derivative, $\frac{\partial C_m}{\partial \left(\frac{qd}{V}\right)} + \frac{\partial C_m}{\partial \left(\frac{\dot\alpha d}{V}\right)}$
C_N	normal-force coefficient, $\frac{\text{normal force}}{q_\infty A}$
d	reference length (diameter of cylinder of AGARD model)
g	gravitational constant, 32.15 ft/sec^2

I_x	moment of inertia about the axis of symmetry
I_y	moment of inertia about a transverse axis through the center of gravity
$K_{1,2,3}$	constants in equation (4)
m	mass of model
M	Mach number
p	roll rate about axis of symmetry of model (positive clockwise looking from rear)
q	pitching velocity
q_∞	free-stream dynamic pressure
R	Reynolds number based on d and free-stream conditions
s	true distance along the flight path
t	flight time
V	velocity along flight path
x	range coordinate in direction of flight path
y	horizontal range coordinate perpendicular to x and z axes
z	vertical range coordinate perpendicular to x and y axes
α	angle of attack (in the vertical plane)
α_m	average value of maximum-angle envelope
α_{min}	average value of minimum-angle envelope
α_{rms}	root-mean-square angle of attack, $\sqrt{\frac{1}{x}\int_0^x \bar{\alpha}_R^2 \, dx}$
α_R	small-angle approximation to resultant angle of attack, $\sqrt{\alpha^2 + \beta^2}$
$\bar{\alpha}_R$	resultant angle of attack, $\tan^{-1}\sqrt{\tan^2 \alpha + \tan^2 \beta}$
β	angle of sideslip (in the horizontal plane)
$\eta_{1,2}$	damping exponents in equation (4)
θ	angular displacement measured in the xz plane

ξ dynamic-stability parameter, $C_D - C_{L_\alpha} + \left(\frac{d}{\sigma}\right)^2\left(C_{m_q} + C_{m_{\dot{\alpha}}}\right)$

ρ free-stream air density

σ radius of gyration about a transverse axis through the center of gravity of a model

Φ angle of rotation of range coordinate axes about the x axis

ψ angular displacement measured in the xy plane

$\omega_{1,2}$ rates of rotation of vectors that describe the model oscillatory motion in equation (4)

DATA-REDUCTION SYSTEM

To obtain aerodynamic coefficients from a free-flight test, the basic data necessary for analysis are position of the center of gravity, angular orientation, and time at various points along the trajectory. The earth-fixed orthogonal coordinate system in which these data are desired is shown in figure 1. Other requirements are a knowledge of the mass, moments of inertia, center-of-gravity location, and geometric characteristics of the model, together with the physical properties of the test gas into which the model is fired.

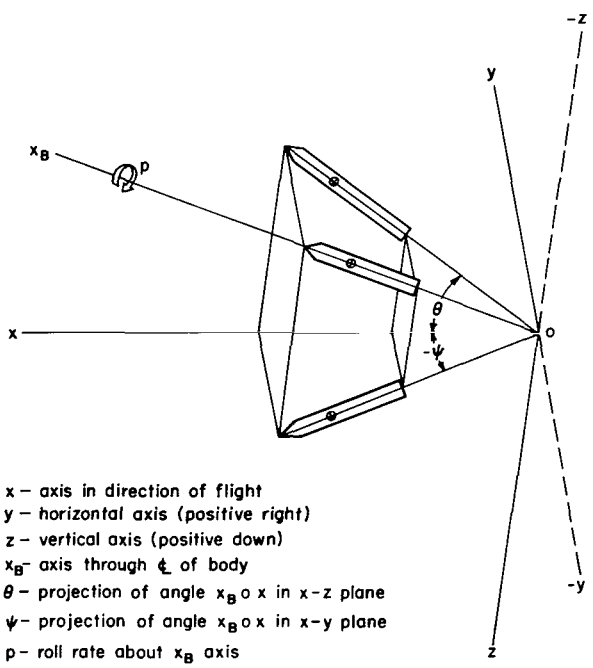

x – axis in direction of flight
y – horizontal axis (positive right)
z – vertical axis (positive down)
x_B – axis through ℄ of body
θ – projection of angle x_B o x in x-z plane
ψ – projection of angle x_B o x in x-y plane
p – roll rate about x_B axis

Figure 1.- Earth-fixed orthogonal coordinate system.

The data-reduction program includes the following routines:

1. Convert raw measurements into earth-fixed orthogonal coordinates

2. Determine drag coefficient and gravity corrections

3. Determine static and dynamic-stability coefficients

4. Rotate orthogonal coordinate system

5. Determine lift coefficients

6. Correct measured angles for flight-path swerve

A description of each of these routines and their dependence on one another will be given.

Obtaining Measurements in Earth-Fixed Orthogonal Coordinate System

The raw measurements obtained from a particular facility must be processed to whatever extent necessary to express them in a set of earth-fixed orthogonal coordinates. This procedure depends on the fiduciary system of the test facility from which the data were obtained and would be bypassed if the data were in the proper coordinates initially.

Drag and Corrections for Gravity

The drag coefficient is obtained directly from the flight time and distance measurements by using a high-precision least-squares curve-fitting procedure (see appendix A). The equation relating time and distance can be written (ref. 4):

$$t = t_o - \frac{1}{V_o K C_D} + \frac{e^{KC_D x}}{V_o K C_D} \tag{1}$$

where $t = t_o$ and $V = V_o$ at $x = 0$ and $K = \rho A/2m$. The parameters C_D, V_o, and t_o are determined to give the "best" fit to the experimental values of x and t. Once these coefficients have been determined, the position and angular measurements in the vertical plane are corrected to account for the influence of gravity. A procedure is also available for eliminating erroneous time measurements (discussed in appendix A).

To this point, the drag coefficient has been assumed to be constant for a given flight (or segment of flight) and not a function of angle of attack. What has been determined is really an effective drag coefficient over the angle-of-attack range encountered in a given flight. From several flights at different amplitudes, the dependence of drag on angle of attack can be determined. For most bodies of revolution, the drag as a function of angle of attack can be expressed as

$$C_D = C_{D_o} + C_1 \bar{\alpha}_R^2 \tag{2}$$

where C_{D_o} is the zero-angle drag coefficient and $\bar{\alpha}_R$ is the resultant angle of attack. It can be shown (ref. 5) that the effective drag coefficient we have determined is

$$C_{D_{eff}} = C_{D_o} + C_1 \alpha_{rms}^2 \tag{3}$$

where

$$\alpha_{rms}^2 = \frac{1}{x} \int_o^x \bar{\alpha}_R^2 \, dx$$

From equations (2) and (3), then, $C_{D_{eff}}$ is the value of C_D that occurs at a resultant angle of attack equal to the root-mean-square resultant angle of attack of the flight in question. Therefore, for each flight or flight segment, one obtains a value for $C_{D_{eff}}$ and α_{rms}. If these points are plotted as $C_{D_{eff}}$ versus α_{rms}^2 and a straight line is fitted to them by least squares, values for C_{D_o} and C_1 are obtained, and one then has an expression for C_D versus angle of attack.

If the drag coefficient cannot be expressed as a quadratic function of angle of attack but is, instead, of the form $C_D = C_{D_o} + C_2|\alpha_R|^n$, then the angle of attack at which the effective drag coefficient should be plotted is

$$\bar{\alpha} = \left(\frac{\int_o^x |\bar{\alpha}_R|^n dx}{x} \right)^{1/n}$$

and

$$C_{D_{eff}} = C_{D_o} + C_2 \bar{\alpha}_R^n \qquad \text{(ref. 6)}$$

The best value of n is found by a trial-and-error process.

Static and Dynamic Stability

Stability coefficients are determined from the oscillatory history of the model. The well-known tricyclic equation derived by Nicolaides (ref. 7), modified to use distance rather than time as the independent variable, is used to analyze the angular motion (see appendix B). Distance is used as the independent variable because it essentially eliminates (to terms of second order) the dependence of the calculations on velocity variation and hence is more convenient. The important assumptions of this method are linear aerodynamics; small angles; constant roll rate; small asymmetries, mass and configurational; and small velocity change. The modified equation is

$$\beta + i\alpha = K_1 e^{(\eta_1 + i\omega_1)x} + K_2 e^{(\eta_2 - i\omega_2)x} + K_3 e^{ipx} \qquad (4)$$

where

$$K_1 = b_1 + ia_1$$

$$K_2 = b_2 + ia_2$$

$$K_3 = b_3 + ia_3$$

$$p = (\omega_1 - \omega_2)(I_y/I_x)$$

A least-squares procedure using differential corrections (ref. 8) is used to fit equation (4) to the experimental data, α and β. The ten constants b_1, a_1,

b_2, a_2, b_3, a_3, η_1, ω_1, η_2, and ω_2 are determined from the fit. As shown in appendix B, when the Magnus moments can be ignored (generally, the case for most ballistic-range tests unless the model is deliberately spun), the constants η_1, η_2, ω_1, and ω_2 are related as follows:

$$\frac{\omega_1}{\omega_2} = \frac{\eta_1 + (\rho A/2m)C_{L_\alpha}}{\eta_2 + (\rho A/2m)C_{L_\alpha}} \tag{5}$$

where C_{L_α} is the lift-curve slope. Because ω_1 and ω_2 are easier to determine accurately, η_2 can be written as a function of η_1, ω_1, and ω_2, thereby reducing the number of unknown coefficients to nine (C_{L_α} must be known and its determination will be discussed later). If p (the roll rate of the model about its own axis, assumed constant) can be measured in flight, ω_1 and ω_2 are not independent of one another and the number of coefficients is reduced to eight. The aerodynamic parameters of static and dynamic stability are related to the determined coefficients as follows: The quasi-linear pitching-moment-curve slope, $C_{m_{\alpha_l}}$, is related to ω_1 and ω_2 as

$$C_{m_{\alpha_l}} = \frac{-2I_Y}{\rho A d}\omega_1\omega_2 \tag{6}$$

and the dynamic-stability parameter, ξ, where $\xi = C_D - C_{L_\alpha} + (d/\sigma)^2(C_{m_q} + C_{m_{\dot{\alpha}}})$ (ref. 9) is related to η_1 and η_2 as

$$\xi = \frac{\eta_1 + \eta_2}{\rho A/2m} \tag{7}$$

The remaining six coefficients, a_i and b_i, along with η_1 and η_2, describe the envelope of oscillatory motion for the particular flight being analyzed.

The assumption of linear aerodynamics, that is, static forces and moments that vary linearly with angle of attack and dynamic forces and moments that vary linearly with angular rates, does not prevent the use of the method for bodies with nonlinear stability coefficients. In such cases, the method is used to reduce data from several flights or portions of flights at different amplitudes. These quasi-linear values for various angle-of-attack amplitudes are then used to obtain the desired coefficients as functions of angle of attack. The method of obtaining nonlinear pitching moments from quasi-linear data is derived in reference 10 and illustrated in some detail in reference 11. Basically, for a pitching-moment equation of the form

$$-C_m = p_0\alpha + p_1\alpha^2 + p_2\alpha^3 + p_3\alpha^4 + p_4\alpha^5 + p_5\alpha^6 + p_6\alpha^7 \cdots \tag{8}$$

the equation for the quasi-linear value of the pitching-moment-curve slope, $C_{m_{\alpha_l}}$, can be written

$$-C_{m_{\alpha_l}} = p_o + \frac{8}{3} p_1 b + \frac{3}{4} p_2 c + \frac{8}{5} p_3 d + \frac{1}{12} p_4 e + \frac{8}{7} p_5 f + \frac{5}{32} p_6 g \cdots \quad (9)$$

where

$$b = \frac{\frac{\alpha_m^5 + \alpha_{min}^5}{2} - \left(\frac{\alpha_m^2 + \alpha_{min}^2}{2}\right)^{5/2}}{(\alpha_m^2 - \alpha_{min}^2)^2}$$

$$c = \alpha_m^2 + \alpha_{min}^2$$

$$d = \frac{\frac{\alpha_m^7 + \alpha_{min}^7}{2} - \left(\frac{\alpha_m^2 + \alpha_{min}^2}{2}\right)^{7/2}}{(\alpha_m^2 - \alpha_{min}^2)^2}$$

$$e = 7\alpha_m^4 + 10\alpha_m^2\alpha_{min}^2 + 7\alpha_{min}^4$$

$$f = \frac{\frac{\alpha_m^9 + \alpha_{min}^9}{2} - \left(\frac{\alpha_m^2 + \alpha_{min}^2}{2}\right)^{9/2}}{(\alpha_m^2 - \alpha_{min}^2)^2}$$

$$g = 3\alpha_m^6 + 5\alpha_m^4\alpha_{min}^2 + 5\alpha_m^2\alpha_{min}^4 + 3\alpha_{min}^6$$

and α_m and α_{min} are the average maximum and minimum resultant angles, respectively, in the α-β plane (sketch (a)).

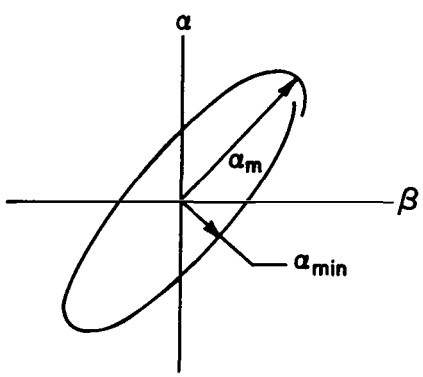

Sketch (a)

Values for $C_{m_{\alpha_l}}$, α_m, and α_{min} from several flights are fitted by a least-squares procedure using as many terms of equation (9) as desired (a computer program has been written to accomplish this systematically (ref. 11)), and the resulting coefficients p_o, p_1, p_2, $\cdots$, etc., are determined. These coefficients then produce an expression for C_m versus α. A method is also available to determine nonlinear results for the dynamic-stability parameter (ref. 12). It has been the author's experience, however, that the quasi-linear values for dynamic stability cannot be determined accurately enough to define the nonlinear contribution.

Rotation of Orthogonal Coordinate System

One of the assumptions necessary in the derivation of equation (4) is that angular displacements are small and that the resultant angle of attack is simply the square root of the sum of the squares of the pitch and yaw angles:

$$\alpha_R = \sqrt{\alpha^2 + \beta^2} \tag{10}$$

The exact expression for the resultant angle of attack is

$$\bar{\alpha}_R = \tan^{-1}\sqrt{\tan^2\alpha + \tan^2\beta} \tag{11}$$

These two equations agree closely for small angles. They agree exactly if α or β equals zero. Thus, the error introduced by equation (10) can be reduced for nearly planar motions by rotating the coordinate axes through an angle Φ so that the motion occurs near either the pitch plane or the yaw plane, thus keeping the angles in the other plane small (see fig. 2). The procedure for rotating the data is described in detail in appendix D.

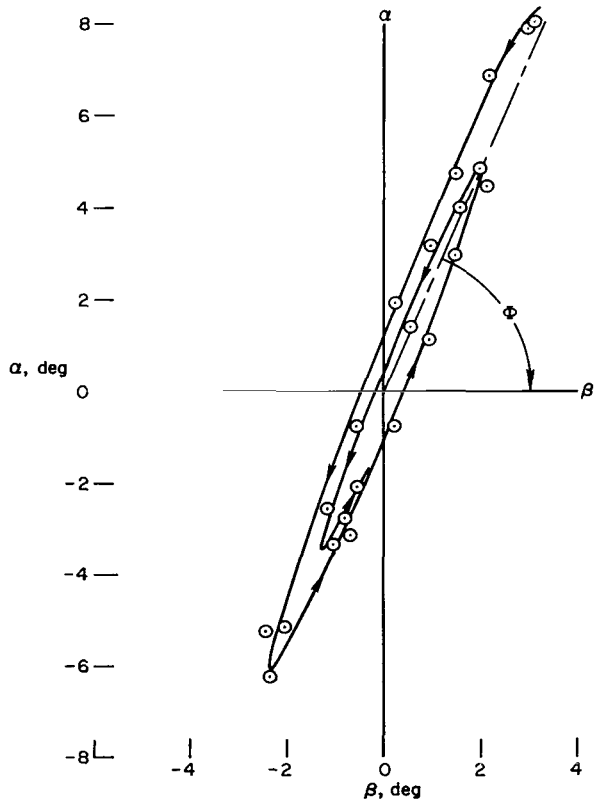

Figure 2.- Rotation of coordinate axes.

The error due to use of equation (10) for large-amplitude motions is most pronounced in the dynamic-stability parameter ξ. Figure 3 (reproduced from ref. 13) demonstrates the magnitude of errors encountered for a typical case. We consider a test in a range having 11 data stations at

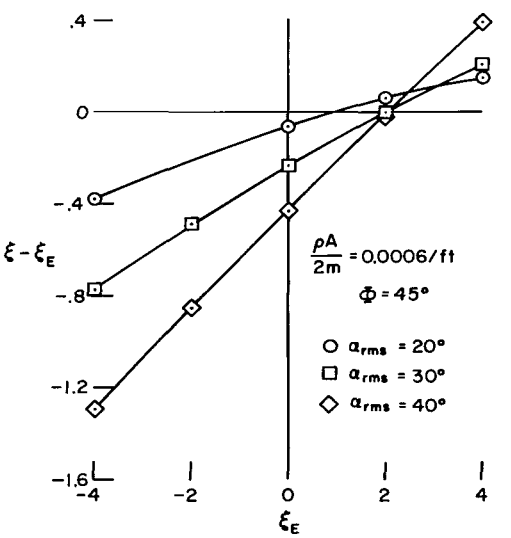

Figure 3.- Effect of resultant angle assumption on dynamic stability parameter.

4-foot intervals with test conditions such that $\rho A/2m = 0.0006/ft$ and the wavelength of oscillatory motion is 26 feet. We consider various values of α_{rms}, Φ, and ξ. Figure 3 shows the induced error ($\xi - \xi_{exact}$) for $\Phi = 45^{\circ}$ (the worst case) as a function of ξ for three values of α_{rms}. Note the near linear dependence of the induced error on ξ, and also the strong influence of α_{rms}.

Lift

The lift-curve slope, C_{L_α}, is determined from swerve measurements (with effects of gravity removed) in conjunction with the oscillatory motion of the model. A modified form of Nicolaides' equation is fitted by the method of least squares to the experimental displacement data z and y. The equation used is (see appendix C for derivation)

$$y + iz = -\frac{\rho A}{2m}\left\{C_{L_\alpha}\int_o^x\int_o^x(\beta + i\alpha)dx\,dx + (d)\left(C_{L_q} + C_{L_{\dot{\alpha}}}\right)\left[\int_o^x(\beta + i\alpha)dx - (\beta_o + i\alpha_o)x\right]\right.$$
$$\left. + (C_{y_o} + iC_{L_o})\left(\frac{1 + ipx - e^{ipx}}{p^2}\right)\right\} + (y_o' + iz_o')x + (y_o + iz_o) \qquad (12)$$

The integrals are obtained in closed form by integrating the tricyclic equation for $\beta + i\alpha$ using the coefficients solved for in the stability routine. Therefore, the constants C_{L_α}, $(C_{L_q} + C_{L_{\dot{\alpha}}})$, C_{y_o}, C_{L_o}, y_o', y_o, z_o', and z_o appear in a linear fashion, and a straightforward least-squares technique can be used to determine them.

Although so far most data have been reduced only for linear lift coefficients, it is fairly straightforward to include suspected nonlinearities. For example, if the lift curve can be approximated by

$$C_L = C_{L_\alpha}\alpha + C_{L_2}\alpha^3$$

one additional term should be added to the right side of equation (12), namely (ref. 13),

$$-\frac{\rho A}{2m}C_{L_2}\int_o^x\int_o^x|\beta + i\alpha|^3\,dx\,dx$$

The additional constant also appears linearly and can be solved for as before.

Corrections to Measured Angles for Flight-Path Curvature

Because the original angular measurements are made with respect to earth-fixed axes and not to the actual flight path, a correction to the angular

data may be required for the swerving of the trajectory as derived from the first pass through the lift routine. Figure 4 shows the relationship of the

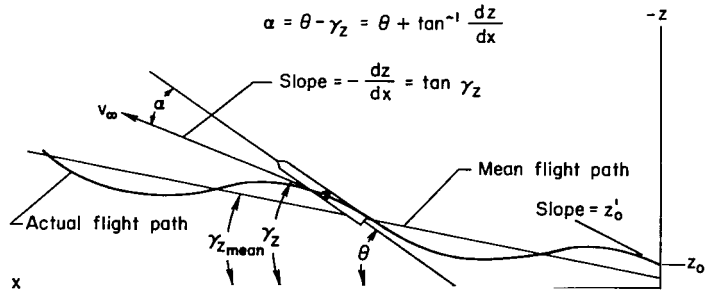

(a) Vertical plane.

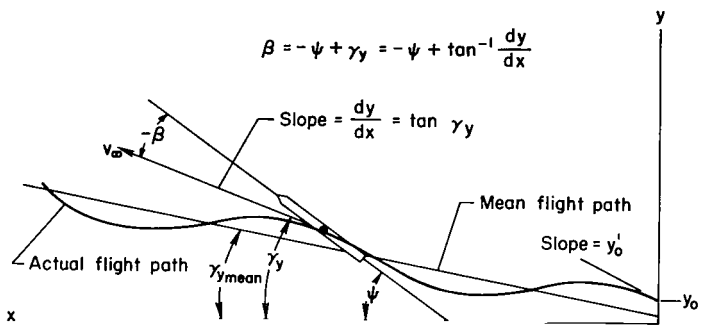

(b) Horizontal plane.

Figure 4.- Relationship of swerve corrections and original measured angles in vertical and horizontal planes.

swerve trajectory, flight-path angle, and measured angles in orthogonal planes. A detailed description of angular corrections is outlined in appendix E. Once this correction is made, the data are again cycled through the stability routine with the corrected measured angles, and this process of recycling continues until the swerve corrections to the angles remain essentially constant.

Program Summary

When the individual routines are completed, a final tabulation of the calculated angles and displacements along with the computation of the root-mean-square angle of attack, α_{rms} (necessary for representing the drag coefficients), is made for a predetermined array of x values that can be used for plotting and reference.

A typical procedure for reducing a free-flight run can be summarized as follows (see fig. 5 for flow chart):

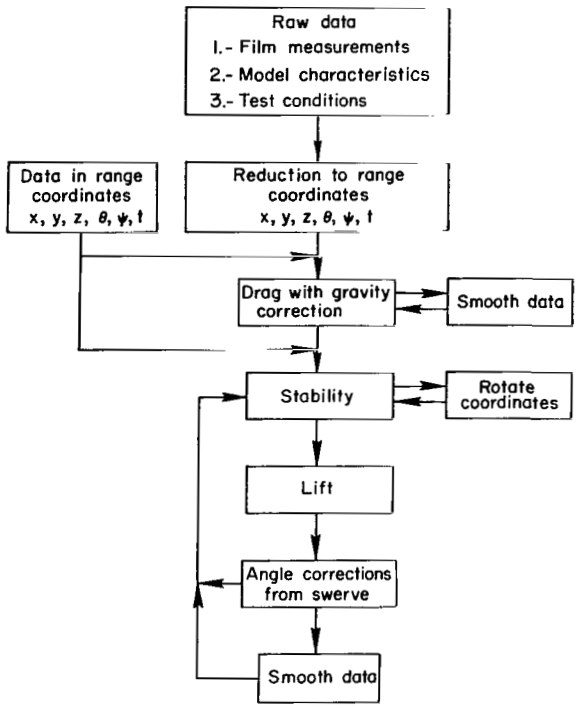

Figure 5.- Flow chart of data reduction procedure.

1. Obtain measurements in earth-fixed, orthogonal coordinates.

2. Fit the x-t data with equation (1) and determine the drag coefficient. Check for bad time data with a smoothing routine and recalculate the drag coefficient if necessary. With time now given as a function of x, compute the vertical drop of the model due to gravity and modify the z and θ measurements to eliminate its effect.

3. Use the θ, ψ, and x data in the stability program to determine the orientation angle (Φ) of the motion with respect to the xy plane.

4. Rotate the θ, ψ, z, and y values through the angle Φ so that the motion occurs as much as possible in the xy plane.

5. Rerun the θ, ψ, and x values through the stability routine to obtain the first set of calculations for the constants in equation (4).

6. Use the y, z, and x data in the lift program along with the computed coefficients from the stability routine, and determine the constants in equation (12).

7. With this set of constants from the lift program, one now has expressions for z versus x and y versus x, which can be differentiated with respect to x to obtain corrections to θ and ψ and thus to estimate α and β.

8. With this new set of angles, the stability program is called again and steps 5 through 7 are repeated until the computed angle corrections are essentially constant. One then has the best fit to the actual oscillatory history with respect to the flight path.

9. At this point the α, β, z, and y data may be checked for data points that appear to be incorrect (appendix F). If any are found, the values are replaced by calculated values and the process of iteration between stability and lift routines is repeated as before.

10. All measured and calculated values for α, β, z, and y are finally rerotated to the original axis system of reference.

The program offers a degree of flexibility to the user; that is, some of the procedures can be done independently of the others, such as the drag routine. The rotation and swerve correction routines are optional as well as the smoothing routines for eliminating bad data. The lift routine can be run independently if one provides the necessary coefficients from the stability analysis of the angular motion. The computing time to reduce one run or run segment is typically 0.5 min on an IBM 7094. Other minor but very convenient (and sometimes necessary) features can be utilized with the program. Additional details of the program are available on request. (Write to Ames Research Center, NASA, Code SVH, Moffett Field, California 94035).

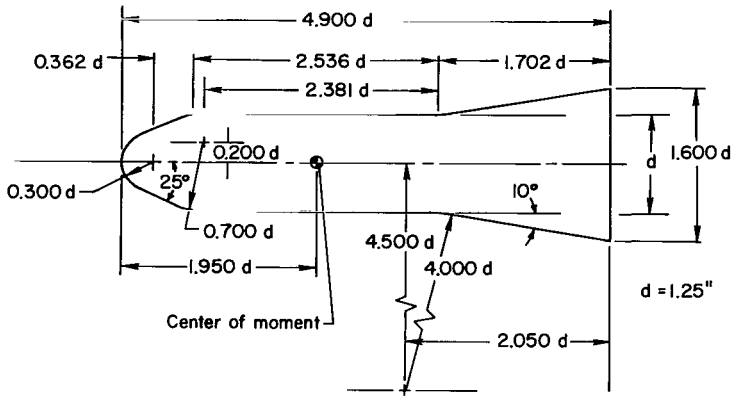

(a) Configuration.

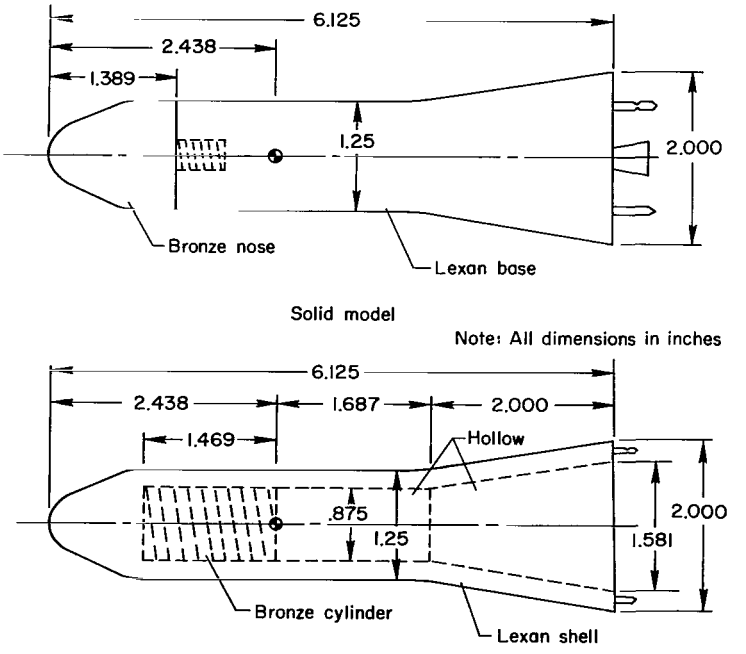

(b) Two types of models.

Figure 6.- Sketch of model.

COMPARISON OF FREE-FLIGHT AND WIND-TUNNEL RESULTS

Tests were conducted at a Mach number of 2.0 and a Reynolds number of 1.7 million in the Ames Pressurized Ballistic Range with the AGARD standard hypersonic ballistic correlation model HB-2 (see fig. 6). Where possible, the results are compared with results obtained in a conventional wind tunnel (refs. 1 and 2) and with results from ballistic-range tests (ref. 14).

The two types of models used in the Ames tests are shown in figure 6(b). The first set of models was solid in construction and was made of phosphor bronze and a polycarbonate-type plastic (Lexan). A second set of models of the same materials was constructed to have a smaller mass and transverse moment of inertia in an unsuccessful attempt at obtaining high angles of attack. This set of models had a hollowed flare and cylinder section as shown. Two pins were mounted

in the base of both sets of models to permit the measurement of roll in flight; therefore, the roll rate was a fixed input to the data-reduction program.

The data used for comparison with wind-tunnel results will be that obtained from the solid models. (The data for all the tests are given in table I.) To reduce the effects of aerodynamic nonlinearities with angle of attack, the data were analyzed with all flights split into overlapping segments of approximately 1-1/2 cycles of motion with three amplitude peaks. Figure 7 shows a typical set of position, time, and angle data for the present tests. Figure 7(a) shows the flight time as a function of distance and the resulting velocity decrease over the length of the range. Figures 7(b) and (c) show the displacement and angular measurements (z and θ were corrected for gravity).

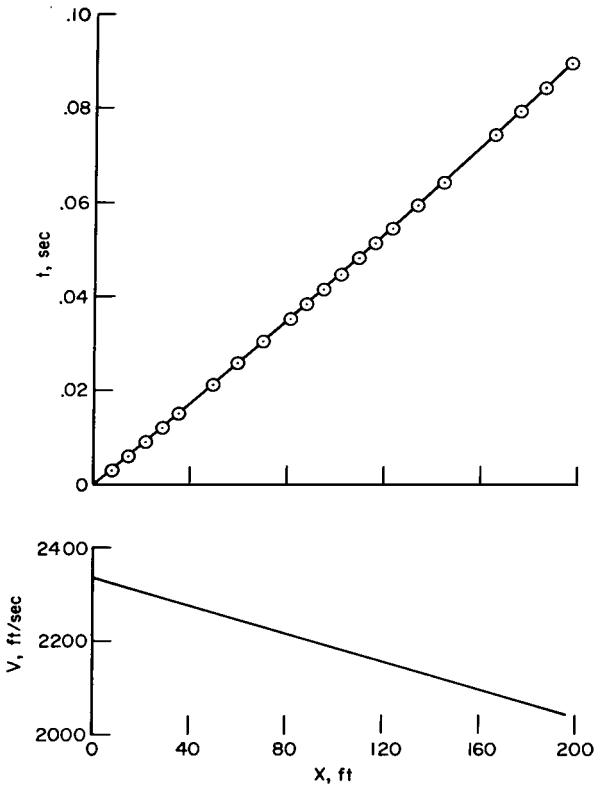

(a) Time and velocity vs. distance.

Figure 7.- Typical flight data.

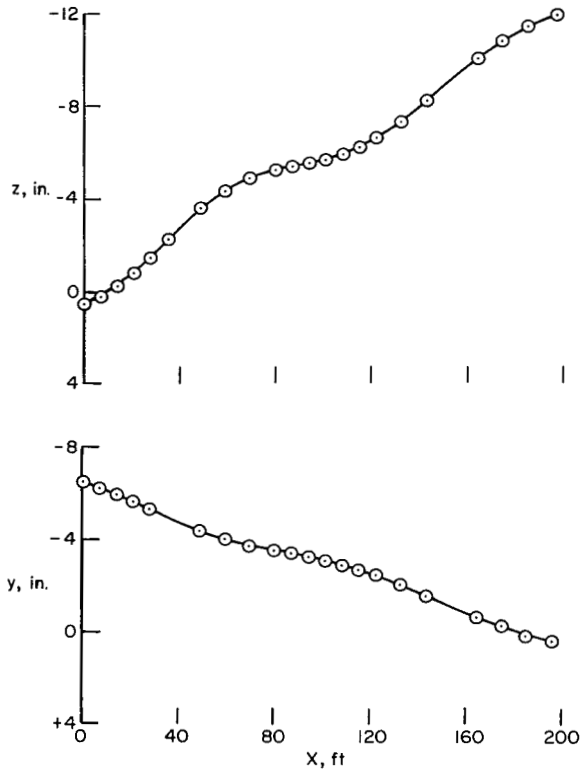

(b) Displacement vs. distance.

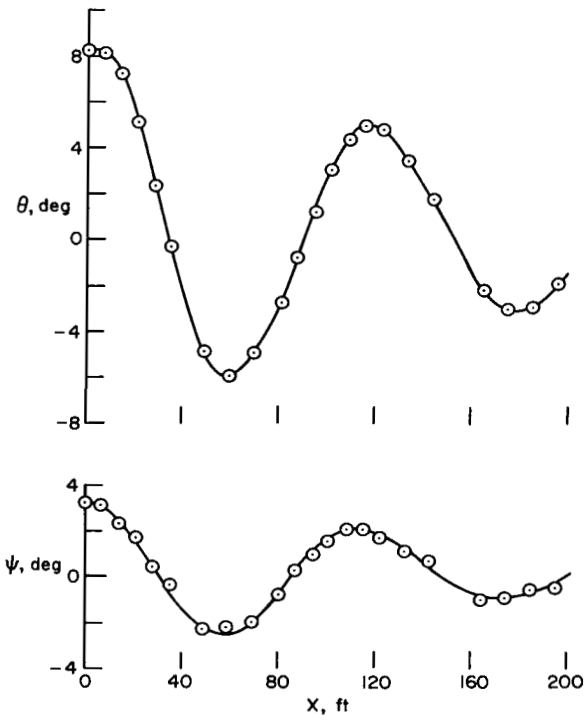

(c) Angular measurements vs. distance.

Figure 7.- Concluded.

Estimate of Error

A method for computing the effects of random errors on the various aerodynamic parameters measured in a ballistic range is outlined in reference 13. With the equations contained therein, estimates of the standard deviation in the respective parameters due to experimental error were made assuming a uniform error distribution with maximum random errors in the measured data of $(\alpha,\beta) = \pm 0.2^{\circ}$, $(x,y,x) = \pm 0.001$ ft, and $(t) = \pm 1 \times 10^{-6}$ sec.

	$\alpha = 2^{\circ}$	$\alpha = 6^{\circ}$
$SD(C_D)$	±0.005	±0.005
$SD(C_{L_\alpha})$	±.3	±.1
$SD(C_{m_{\alpha_l}})$	±.009	±.003
$SD(\xi)$	±.6	±.2

Drag

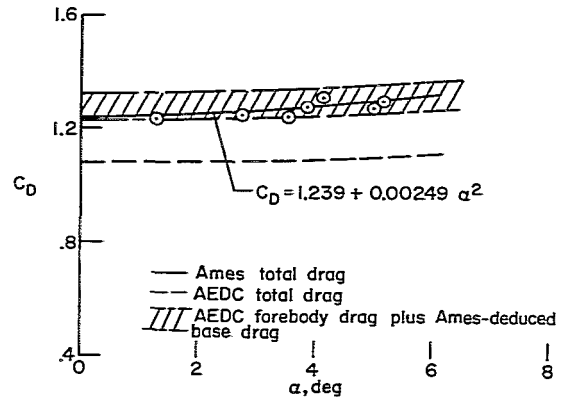

Figure 8.- Variation of drag coefficient with angle of attack.

The total drag coefficient as a function of angle of attack is shown in figure 8.[2] Each data point was obtained by analyzing a flight (or portion of flight) as already outlined. These data points were then fitted by a quadratic equation in angle of attack by the method of least squares. One immediately notices the significant difference between the present ballistic-range results and AEDC wind-tunnel results. The total drag for the wind-tunnel results was obtained by combining the contributions of forebody and base drag measurements given in reference 1. It was felt that the discrepancy could be in the wind-tunnel base pressure measurements since sting effects on these measurements have been shown to be significant. In reference 15, the effect of sting size on base pressure measurements for a 15° half-angle cone was investigated. Three different ratios of sting diameter to model base diameter were investigated and the results were compared with the measurements obtained for "no sting" on a free-flight model with a pressure transducer coupled to an FM telemetry system. This investigation revealed that for sting-to-model-diameter ratios as low as 0.3, as was used in the AEDC tests of the AGARD model, the base pressure measurements could be as much as 70 percent too high, thereby producing a lower total drag coefficient. In view of these facts, then, it was decided to attempt to deduce the base pressure on the present free-flight models from shadowgraphs of the model in flight. An orthogonal set of shadowgraphs was selected from each of the four flights with an angle of attack of approximately zero in each plane of view. A typical shadowgraph is shown in figure 9.[3] The expansion of the flow around the base and the wake are well defined. If one measures the Mach angle between the final Mach line at the corner of the base and the dividing streamline defining the outer edge

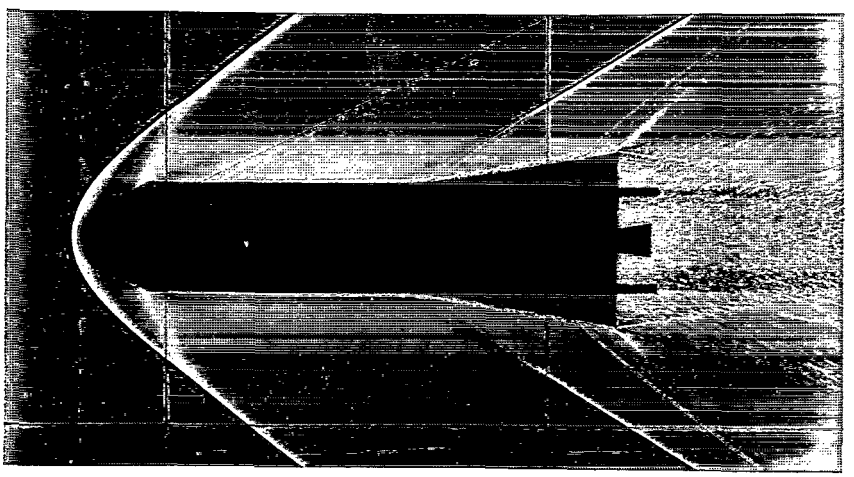

Figure 9.- Shadowgraph of model; M = 2.06, R = 1.85×10^6.

[2]Most of the scatter in the data points can be attributed to slight differences in Mach number. In table I, the drag coefficient increases slightly with a decrease in Mach number for a given range of α_{rms}.

[3]The intense shock pattern shown on the last half inch of the model is the area where the sabot gripped the model.

of the wake, the Mach number of the flow along the wake can be determined and, consequently, the ratio of static-to-total pressure in the wake (and on the base) is known. The total pressure behind the normal shock at the nose is assumed to be constant everywhere on the body and, as a result, the ratio of static pressure at the base to free-stream pressure is known. The base drag can then be calculated. The calculated values from all four flights were averaged and added to the AEDC forebody drag; the shaded curve shown in figure 8 is the result. The total deviation from the average base drag is indicated by the shaded error band. The agreement with the free-flight total drag is now excellent.

Lift

The lift-curve slope, as deduced from the swerving motion of the model, is shown in figure 10. These data indicate that the lift coefficient is linear with angle of attack at least to 7°. The wind-tunnel result for lift-curve slope, as deduced from the normal and axial force measurements, is shown, together with a value obtained using the Ames deduced base pressure in the axial force contribution. The agreement between free-flight and wind-tunnel results is very good.

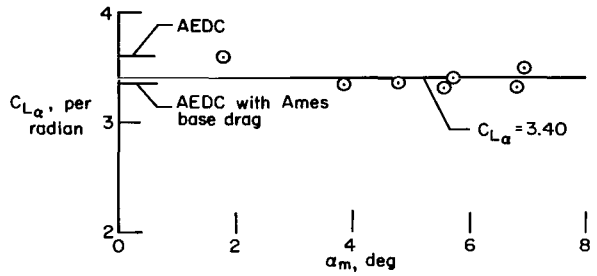

Figure 10.- Lift-curve slope.

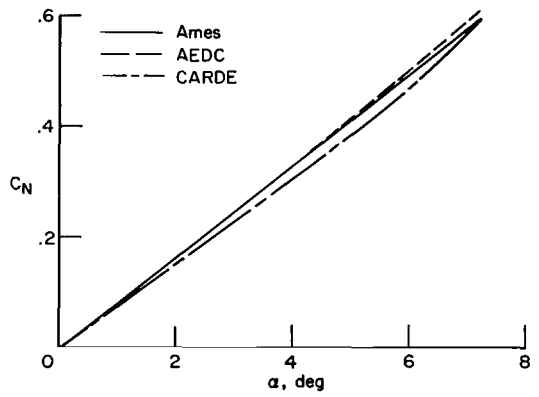

Figure 11.- Variation of normal-force coefficient with angle of attack.

Normal Force

A curve of normal force versus angle of attack was calculated from the measured lift and drag data where $C_L = 3.40\alpha$ and $C_D = 1.239 + 0.00249\alpha^2$ and $C_N = C_L \cos \alpha + C_D \sin \alpha$. The results are plotted in figure 11 and are compared with AEDC wind-tunnel data and with CARDE ballistic-range data (ref. 14).

Pitching Moment

The nonlinear pitching-moment-coefficient curve was calculated with the method of reference 9, with linear and cubic terms in angle of attack chosen as most representative of the data. (Higher order polynomials were examined, but were nearly identical to the simpler linear-cubic representation.) One flight at low amplitude ($\alpha_m = 1.8°$) revealed a significant decrease in static stability (see table I, run 1156), which is reflected in the lower initial slope of the pitching-moment curve in

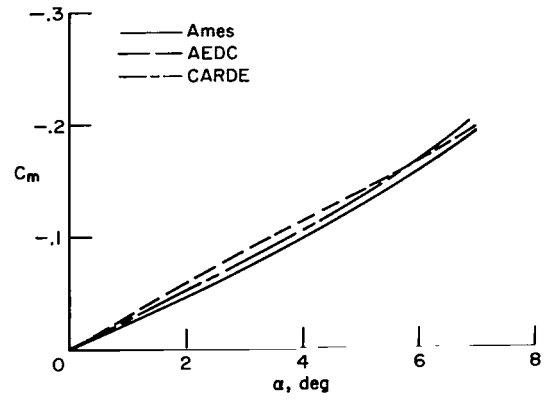

Figure 12.- Variation of pitching-moment coefficient with angle of attack.

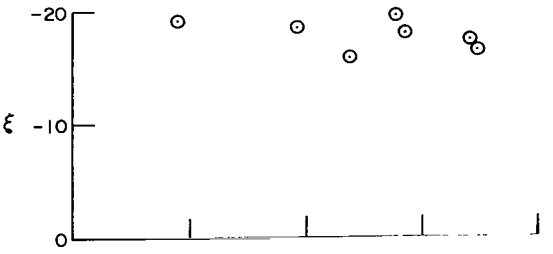

(a) Dynamic stability parameter.

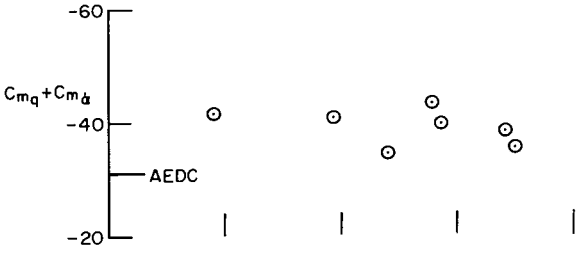

(b) Damping in pitch.

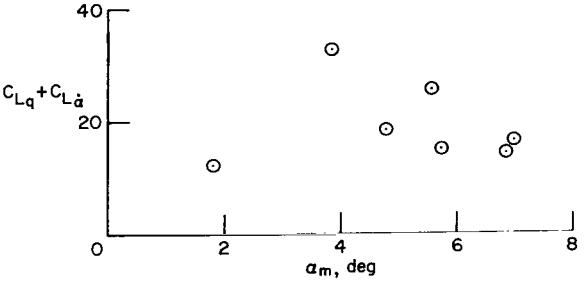

(c) Lift due to pitching and plunging.

Figure 13.- Variation of dynamic aerodynamic coefficients with angle of attack.

figure 12. Curves from AEDC and CARDE are also shown and indicate slightly higher values for the pitching moment. Small differences in boundary-layer conditions and base pressure could contribute to the discrepancy.

Dynamic Stability

The dynamic-stability parameter for nonpowered flight at constant altitude, $\xi = C_D - C_{L_\alpha} + (d/\sigma)^2(C_{m_q} + C_{m_{\dot{\alpha}}})$, is shown in figure 13(a) and the resulting values for $(C_{m_q} + C_{m_{\dot{\alpha}}})$ in figure 13(b). The value of $(C_{m_q} + C_{m_{\dot{\alpha}}})$ obtained in conventional wind-tunnel tests (ref. 2) is slightly lower than free-flight results. The dynamic contribution to lift due to pitching and plunging $(C_{L_q} + C_{L_{\dot{\alpha}}})$, which can also be considered as the contribution to damping in pitch due to lift (other major contributions would be center-of-pressure movement or changes in drag due to angular rates), is shown in figure 13(c). To the author's knowledge, this is the first fairly consistent set of data obtained for $(C_{L_q} + C_{L_{\dot{\alpha}}})$ in a ballistic range.

Effects of Hollow-Base Models

While, as noted earlier, the attempt to obtain higher angles of attack by reducing the mass and transverse moment of inertia of the models was not successful, the data from this set of tests revealed some interesting results. Figure 14 shows the drag coefficient for both solid and hollow-base models. Although some of the scatter in the data for each model type can be attributed to slight Mach number effects, the hollow-base models had a slightly lower overall drag coefficient than the solid models. The reason for the lower drag is not known but may be due to subtle boundary-layer differences or effects of the hollow base or both.

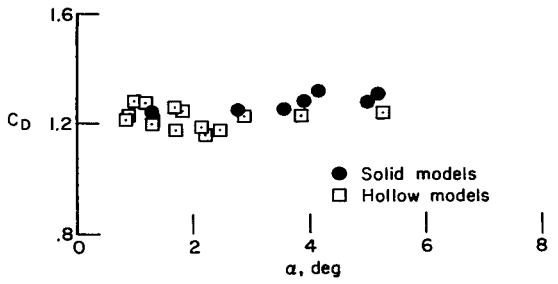

Figure 14.- Drag measurements for solid and hollow-base models.

Data for the other aerodynamic parameters for the hollow models were very similar to data for the solid models except that there seemed to be more scatter. It is possible that the open-base creates a "sloshing" effect of the air movement in that vicinity and may introduce slight differences in the forces and moments. It should be pointed out that an open-base model was used in the CARDE tests, but the envelope of oscillatory motion for the tests never reached below approximately 7° and therefore might not be sensitive to these effects. Model base geometry should be carefully considered in the design of models for tests at subsonic and moderate supersonic Mach numbers at which base pressure is comparable to the free-stream pressure and the base forces are comparable to forebody forces.

Ames Research Center
National Aeronautics and Space Administration
Moffett Field, Calif. 94035, May 16, 1968
124-07-02-35-00-21

APPENDIX A

DRAG COEFFICIENT AND GRAVITY CORRECTION SUBROUTINE

The purpose of this subroutine is twofold. First, it obtains a least-squares fit of the drag equation to a set of measurements of distance flown as a function of time to deduce a drag coefficient. Second, the drag equation is then used to calculate corrections to the displacement and angle measurements in the vertical plane to obtain a zero gravity trajectory.

Drag

The equation of motion along the flight path is

$$m \frac{d^2s}{dt^2} = D = - \frac{\rho A}{2} C_D \left(\frac{ds}{dt}\right)^2 \tag{A1}$$

where D is the drag and s is the distance traveled by the model center of gravity. The present analysis is based on the following assumptions:

1. The distance s can be replaced by x, the distance along the earth-fixed axis in the direction of flight. This assumption is very good since the lateral motion is small compared to the motion in the x direction.

2. The air density, ρ, the model mass, m, the reference area, A, and the drag coefficient, C_D, are constant.[1]

With these assumptions and the initial conditions $t = t_o$ and $V = V_o$ at $x = 0$ the solution to equation (A1) is

$$t = t_o - \frac{1}{V_o K C_D} + \frac{e^{KC_D x}}{V_o K C_D} \tag{A2}$$

where $K = \rho A/2m$ and the subscript o denotes initial conditions.

To obtain a least-squares fit to the x and t data, we write equation (A2) as

$$t = Ae^{Cx} + B \tag{A3}$$

[1]In most tests the velocity loss during flight is small; hence, changes in drag coefficient because of diminishing Reynolds number or Mach number may usually be neglected. (This may not be true in transonic tests or, to a small degree, in the present tests.) In most cases, however, the drag coefficient is a strong function of angle of attack. This point is considered in the text and a method for determining the variation with angle of attack is given.

where

$$A = \frac{1}{V_o K C_D}$$

$$B = t_o - \frac{1}{V_o K C_D}$$

$$C = K C_D$$

We will now set up the least-squares procedure. The sum of the squares of the residuals, SSR, is written

$$SSR = \sum_{i=1}^{N} (t_{exp_i} - t_i)^2 W_i \tag{A4}$$

where t_{exp_i} is the experimentally determined time at the ith position, t_i is the calculated time, W_i is a weighting factor, and the summation extends over all positions N. (The normal mode is to operate with a W_i of 1; however, one can use 0 as a mechanism for rejecting erroneous data points.) Substituting equation (A3) into (A4) yields

$$SSR = \sum_{i=1}^{N} (t_{exp_i} - Ae^{Cx_i} - B)^2 W_i \tag{A5}$$

The normal least-squares procedure would be to form the partial derivatives of equation (A5) with respect to A, B, and C and set them equal to zero, and solve for A, B, and C. This works as long as the partial derivatives are linear in the unknown coefficients, but it does not work here because C appears in an exponent. Hence, we will proceed as follows: Form the partials with respect to A and B and set them equal to zero, yielding

$$\frac{\partial SSR}{\partial A} = -2 \sum_{i=1}^{N} W_i (t_{exp_i} - Ae^{Cx_i} - B) e^{Cx_i} = 0 \tag{A6}$$

$$\frac{\partial SSR}{\partial B} = -2 \sum_{i=1}^{N} W_i (t_{exp_i} - Ae^{Cx_i} - B) = 0 \tag{A7}$$

Using equations (A6) and (A7) eliminate A and B from equation (A5) to yield

$$SSR = \sum_{i=1}^{N} \left(\left\{ t_{exp_i} + \left[\frac{\left(\sum W_i\right)\left(\sum W_i t_{exp_i} e^{Cx_i}\right) - \left(\sum W_i t_{exp_i}\right)\left(\sum W_i e^{Cx_i}\right)}{\left(\sum W_i e^{Cx_i}\right)^2 - \left(\sum W_i\right)\left(\sum W_i e^{2Cx_i}\right)} \right] e^{Cx_i} \right.$$

$$\left. - \left[\frac{\left(\sum W_i e^{Cx_i}\right)\left(\sum W_i t_{exp_i} e^{Cx_i}\right) - \left(\sum W_i t_{exp_i}\right)\left(\sum W_i e^{2Cx_i}\right)}{\left(\sum W_i e^{Cx_i}\right)^2 - \left(\sum W_i\right)\left(\sum W_i e^{2Cx_i}\right)} \right] \right\}^2 W_i \Bigg) \tag{A8}$$

We now have an equation in C only. At this point, a differential correction procedure (ref. 13) could be used, but the partial derivative with respect to C would be quite complicated. Therefore, a numerical procedure is used to minimize the SSR as follows: An approximate solution for C_D and hence C is found (to be discussed in the next paragraph), and equation (A8) is evaluated. Then the value of C_D is increased by ϵ (e.g., $\epsilon = 0.1\ C_D$) and equation (A8) is reevaluated. If the SSR is smaller than the first value, C_D is increased by ϵ again, continuing until the minimum in SSR is passed, at which point the size of ϵ is reduced by one-half and C_D decreased by ϵ. This process is repeated until the minimum is passed again, at which point ϵ is again reduced by one-half and C_D increased by ϵ. This process is repeated until C_D changes less than some prescribed amount. Normally, a value of 1 percent of the last value of C_D obtained is used. If, by chance, the first step had produced an increase in SSR, the direction would have been changed. Equation (A8) is evaluated to find SSR in double-precision arithmetic to insure accurate determination of the minimum.

The starting solution for the above iteration procedure is found by utilizing the small-velocity-loss criterion, that is, small KC_Dx, and expanding the exponential in equation (A3) to order x^2 to obtain

$$t = (A + B) + ACx + \frac{AC^2}{2} x^2 \tag{A9}$$

or

$$t = \bar{A} + \bar{B}x + \bar{C}x^2 \tag{A10}$$

By least-squares fitting equation (A10) to the x - t data, values of $\bar{A}$, $\bar{B}$, and $\bar{C}$ and, hence, C_D are obtained. The least-squares fitting of (A10) is straightforward since all three unknowns appear in a linear manner.

Gravity Corrections

After convergence of the drag routine, gravity corrections can be calculated. The new vertical position becomes

$$z_{n_i} = z_{exp_i} - \frac{1}{2} g t_i^2 \tag{A11}$$

where z_{n_i} is the new z at the ith position and z_{exp_i} is the experimentally determined z at the ith position, and the curvature of the flight path due to gravity is

$$\left.\frac{dz}{dx}\right|_i = \frac{g t_i}{V_i} \tag{A12}$$

Hence, the new angular coordinate is

$$\theta_{n_i} = \theta_{exp_i} + \tan^{-1} \left.\frac{dz}{dx}\right|_i \tag{A13}$$

At this point we may elect to check for erroneous data points as follows: The standard deviation of the time measurements is calculated from the SSR as

$$SD(t) = \sqrt{\frac{SSR}{N}} \tag{A14}$$

Now the difference between the experimental and the calculated time from the least-squares fit is compared to SD(t). If the absolute value of this difference exceeds a chosen multiple of SD(t) (normally taken as 2), the data point is deleted from the set of data. When all data points have been checked, the least-squares procedure is repeated if points were deleted; if points were not deleted, the procedure is finished. When data points are deleted, a statement to this effect is printed in the output.

APPENDIX B

MODIFIED TRICYCLIC EQUATIONS

Nicolaides' differential equation of motion using trajectory-oriented forces rather than body-oriented forces can be expressed in time coordinates as follows:

$$\ddot{\zeta} - V\left(\frac{\rho A}{2m}\left\{-C_{L_\alpha} + \left(\frac{d}{\sigma}\right)^2\left(C_{m_q} + C_{m_{\dot{\alpha}}}\right) + i\,\frac{pd}{V}\left[C_{L_{p_\alpha}} + \left(\frac{d}{\sigma}\right)^2\left(C_{m_{p_{\dot{\alpha}}}} - C_{m_{p_q}}\right)\right]\right\}\right.$$

$$\left. + i\,\frac{p}{V}\,\frac{I_x}{I_y}\right)\dot{\zeta} + V^2\left[-\frac{\rho A d}{2I_y}\left(C_{m_\alpha} + i\,\frac{pd}{V}\,C_{m_{p_\alpha}}\right) + \frac{p}{V}\,\frac{I_x}{I_y}\,\frac{\rho A}{2m}\left(-\frac{pd}{V}\,C_{L_{p_\alpha}} - iC_{L_\alpha}\right)\right]\zeta$$

$$= Q(t)e^{i\int p\,dt} \qquad \text{(B1)}$$

where $\zeta = \beta + i\alpha$ and $m\sigma^2 = I_y$. If we change to x coordinates

$$\dot{\zeta} = \dot{x}\zeta' \qquad \text{(B2)}$$

$$\ddot{\zeta} = \ddot{x}\zeta' + \dot{x}\,\frac{d\zeta'}{dt} = \ddot{x}\zeta' + \dot{x}\,\frac{d\zeta'}{dx}\,\frac{dx}{dt}$$

$$\ddot{\zeta} = \ddot{x}\zeta' + \dot{x}^2\zeta'' \qquad \text{(B3)}$$

Note that

$$\dot{x} \cong V$$

$$\ddot{x} \cong \frac{\rho A}{2m}\,V^2(-C_L\gamma - C_D)$$

where $\gamma = |\gamma_y - i\gamma_z|$ is the local flight-path angle (angle between the local velocity vector and the x axis of the range). (See fig. 4.) For small γ, as is the case in a ballistic range where the velocity vector is nearly parallel to the x axis, the $C_L\gamma$ term can be neglected. Substituting for $\dot{x}$ and $\ddot{x}$ into equations (B2) and (B3) yields

$$\dot{\zeta} = V\zeta' \qquad \text{(B2a)}$$

$$\ddot{\zeta} = V^2\left(\zeta'' - \zeta'\,\frac{\rho A}{2m}\,C_D\right) \qquad \text{(B3a)}$$

Also,

$$p(t) = Vp(x) \tag{B4}$$

Substituting equations (B2a), (B3a), and (B4) for (B1) yields

$$\zeta'' - \left\{\frac{\rho A}{2m}\xi + i\frac{\rho A}{2m}pd\left[C_{L_{p_\alpha}} + \left(\frac{d}{\sigma}\right)^2\left(C_{m_{p_{\dot{\alpha}}}} - C_{m_{p_q}}\right)\right] + ip\frac{I_x}{I_y}\right\}\zeta'$$

$$+ \left[-\frac{\rho Ad}{2I_y}\left(C_{m_\alpha} + ipdC_{m_{p_\alpha}}\right) + p\frac{I_x}{I_y}\frac{\rho A}{2m}\left(-pdC_{L_{p_\alpha}} - iC_{L_\alpha}\right)\right]\zeta = Qe^{ipx} \tag{B5}$$

where

$$\xi = C_D - C_{L_\alpha} + \left(\frac{d}{\sigma}\right)^2\left(C_{m_q} + C_{m_{\dot{\alpha}}}\right)$$

Differential equation (B5) can be written as

$$\zeta'' - (\varphi_1 + \varphi_2)\zeta' + \varphi_1\varphi_2\zeta = K_3(\varphi_3 - \varphi_1)(\varphi_3 - \varphi_2)e^{\varphi_3 x}$$

which has the solution (see sketch (b))

$$\zeta = K_1e^{\varphi_1 x} + K_2e^{\varphi_2 x} + K_3e^{\varphi_3 x} \tag{B6}$$

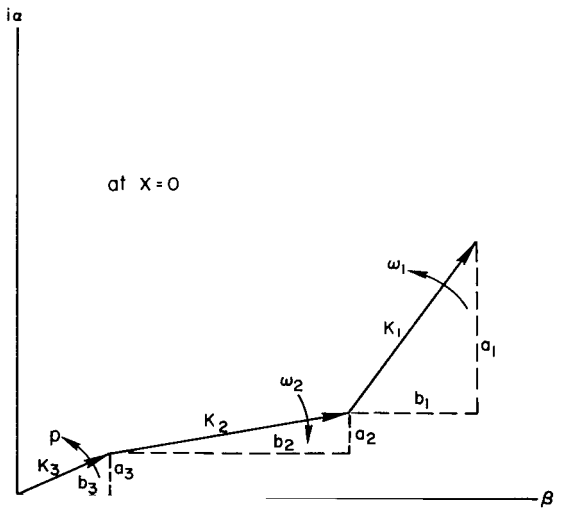

Sketch (b)

where

$\varphi_1 = \eta_1 + i\omega_1$

$\varphi_2 = \eta_2 - i\omega_2$

$\varphi_3 = ip$

$K_1 = b_1 + ia_1$

$K_2 = b_2 + ia_2$

$K_3 = b_3 + ia_3$

Note then that

$$\varphi_1 + \varphi_2 = \frac{\rho A}{2m}\xi + i\left\{pd\,\frac{\rho A}{2m}\left[C_{L_{p_\alpha}} + \left(\frac{d}{\sigma}\right)^2\left(C_{m_{p_{\dot{\alpha}}}} - C_{m_{p_q}}\right)\right] + p\,\frac{I_x}{I_y}\right\}$$

$$\varphi_1\varphi_2 = -\frac{\rho Ad}{2I_y}\left(C_{m_\alpha} + ipdC_{m_{p_\alpha}}\right) + p\,\frac{I_x}{I_y}\,\frac{\rho A}{2m}\left(-pdC_{L_{p_\alpha}} - iC_{L_\alpha}\right)$$

$$K_3(\varphi_3 - \varphi_1)(\varphi_3 - \varphi_2) = Q$$

Also,

$$\varphi_1 + \varphi_2 = \eta_1 + \eta_2 + i(\omega_1 - \omega_2)$$

$$\varphi_1\varphi_2 = \eta_1\eta_2 + \omega_1\omega_2 + i(\eta_2\omega_1 - \eta_1\omega_2)$$

Therefore,

$$\eta_1 + \eta_2 = \frac{\rho A}{2m}\xi \tag{B7}$$

$$\omega_1 - \omega_2 = pd\,\frac{\rho A}{2m}\left[C_{L_{p_\alpha}} + \left(\frac{d}{\sigma}\right)^2\left(C_{m_{p_{\dot{\alpha}}}} - C_{m_{p_q}}\right)\right] + p\,\frac{I_x}{I_y} \tag{B8}$$

$$\eta_1\eta_2 + \omega_1\omega_2 = -\frac{\rho Ad}{2I_y}\,C_{m_\alpha} - p^2d\,\frac{I_x}{I_y}\,\frac{\rho A}{2m}\,C_{L_{p_\alpha}} \tag{B9}$$

$$\eta_2\omega_1 - \eta_1\omega_2 = -p\,\frac{I_x}{I_y}\,\frac{\rho A}{2m}\,C_{L_\alpha} - pd\,\frac{\rho Ad}{2I_y}\,C_{m_{p_\alpha}} \tag{B10}$$

If one neglects Magnus forces and moments and if $\eta_1\eta_2 \ll \omega_1\omega_2$, then

$$\xi = \frac{\eta_1 + \eta_2}{\frac{\rho A}{2m}} \tag{B7a}$$

$$\omega_1 - \omega_2 = p\,\frac{I_x}{I_y} \tag{B8a}$$

$$C_{m_\alpha} = -\frac{2I_y\omega_1\omega_2}{\rho Ad} \tag{B9a}$$

and from equation (B10)

$$C_{L_\alpha} = \frac{\eta_1\omega_2 - \eta_2\omega_1}{p\,\frac{I_x}{I_y}\,\frac{\rho A}{2m}} \tag{B10a}$$

However, the calculated values for η_1, η_2, ω_1, and ω_2 are not precise enough to obtain accurate values of C_{L_α}. A value for C_{L_α} is determined much more accurately from the plunging motion. Once a value of C_{L_α} is obtained, it can then be used to determine η_2 as a function of η_1, ω_1, and ω_2 from equations (B8a) and (B10a). Therefore,

$$\eta_2 = \left(\eta_1 + \frac{\rho A}{2m} C_{L_\alpha}\right) \frac{\omega_2}{\omega_1} - \frac{\rho A}{2m} C_{L_\alpha} \tag{B11}$$

When p is known from experimental measurements, then

$$\omega_2 = \omega_1 - p \frac{I_x}{I_y}$$

consequently,

$$\eta_2 = \left(\eta_1 + \frac{\rho A}{2m} C_{L_\alpha}\right) \frac{\omega_1 - p \frac{I_x}{I_y}}{\omega_1} - \frac{\rho A}{2m} C_{L_\alpha} \tag{B12}$$

and ω_2 and η_2 would be functions only of ω_1 and η_1, and the values of p and C_{L_α}.

The experimental data for α and β are fitted with the tricyclic equation (eq. B6)) by a least-squares procedure using the method of differential corrections (ref. 8). To initiate this procedure, starting values for the unknown coefficients must be provided. This is accomplished by using a modification of Prony's method (ref. 16), which will be described next.

The following theorem is fundamental to Prony's method: If

$$(\beta + i\alpha)_l = \sum_{j=1}^{3} K_j e^{\varphi_j x_l} \tag{B13}$$

where $x = x_1, x_2, \cdots x_n$ (x locations of equally spaced points, Δx apart) and $l = 1, 2, \cdots n$ (n = number of points $(\beta + i\alpha)$). Then $\beta + i\alpha$ satisfies the linear difference equation

$$(\beta + i\alpha)_{l+3} + Q_2(\beta + i\alpha)_{l+2} + Q_1(\beta + i\alpha)_{l+1} + Q_0(\beta + i\alpha)_l = 0 \tag{B13a}$$

where Q are constants such that the roots of

$$h^3 + Q_2 h^2 + Q_1 h + Q_0 = 0 \tag{B14}$$

are

$$h_j = e^{\varphi_j \Delta x}$$

We have thus minimized

$$\sum \left[(\beta + i\alpha)_{l+3} + Q_2(\beta + i\alpha)_{l+2} + Q_1(\beta + i\alpha)_{l+1} + Q_0(\beta + i\alpha)_l \right]^2$$

instead of

$$\sum \left[(\beta + i\alpha)_{\text{measured}} - (\beta + i\alpha)_{\text{calculated}} \right]^2$$

which means simply that the coefficients derived from the procedure are not the best possible coefficients but are very good first approximations. To obtain values for the coefficients K_j and φ_j the following steps would normally be taken: Solve the following set of equations by the method of least squares for Q_2, Q_1, and Q_0. (See eq. (B13a).)

$$(\beta + i\alpha)_4 + Q_2(\beta + i\alpha)_3 + Q_1(\beta + i\alpha)_2 + Q_0(\beta + i\alpha)_1 = 0$$

$$(\beta + i\alpha)_5 + Q_2(\beta + i\alpha)_4 + Q_1(\beta + i\alpha)_3 + Q_0(\beta + i\alpha)_2 = 0$$

$$\vdots$$

$$(\beta + i\alpha)_n + Q_2(\beta + i\alpha)_{n-1} + Q_1(\beta + i\alpha)_{n-2} + Q_0(\beta + i\alpha)_{n-3} = 0$$

With Q_2, Q_1, and Q_0 known, solve the cubic equation

$$h^3 + Q_2 h^2 + Q_1 h + Q_0 = 0$$

for roots h_1, h_2, and h_3 where

$$h_1 = e^{\varphi_1 \Delta x}$$

$$h_2 = e^{\varphi_2 \Delta x}$$

$$h_3 = e^{\varphi_3 \Delta x}$$

Therefore, by solving for φ_1, φ_2, and φ_3 and then substituting them into equation (B13), one can do a second least-squares operation to obtain K_1, K_2, and K_3. However, since φ_3 is not independent of φ_1 and φ_2 for the tricyclic equation in question (i.e., $p = f(\omega_1, \omega_2) \Rightarrow g(\varphi_1, \varphi_2)$), a slight modification is used. The procedure is:

Assume initially that $\varphi_3 = 0$ and thus $h_3 = e^0 = 1$. Therefore

$$(\beta + i\alpha)_l = K_1 e^{\varphi_1 x_l} + K_2 e^{\varphi_2 x_l} + K_3$$

and $h^3 + Q_2 h^2 + Q_1 h + Q_0 = 0$ has unity as a root so that $1 + Q_2 + Q_1 + Q_0 = 0$. If Q_0 is eliminated between this equation and equation (B13a),

$$\left[(\beta + i\alpha)_{l+2} - (\beta + i\alpha)_l\right] Q_2 + \left[(\beta + i\alpha)_{l+1} - (\beta + i\alpha)_l\right] Q_1 = (\beta + i\alpha)_l - (\beta + i\alpha)_{l+3}$$

This equation is now solved by least squares for the coefficients Q_1 and Q_2. The exponentials $e^{\varphi_1 \Delta x}$ and $e^{\varphi_2 \Delta x}$ are now found to be the roots of

$$h^2 + (Q_2 + 1)h + (Q_1 + Q_2 + 1) = 0$$

So, from

$$h_1 = e^{\varphi_1 \Delta x}$$

$$h_2 = e^{\varphi_2 \Delta x}$$

the values of φ_1 and φ_2 are found from which φ_3 is calculated; the process is repeated with a new φ_3 until the coefficients remain essentially constant.

The coefficient $e^{\varphi_j x_l}$ of K_j in equation (B13) is tabulated for each j since φ_j is known. Therefore, K_j can be found by a second least-squares procedure.

The values of α and β provided for this routine are either computed internally directly from the raw angle data with a table look-up-and-interpolation scheme or are input directly with constant increments of distance.

APPENDIX C

LIFT EQUATIONS

If Magnus terms are neglected and if trajectory rather than body-oriented force coefficients are used, Nicolaides' equation for lift can be written as

$$\ddot{y} + i\ddot{z} = -\frac{\rho A}{2m} V^2 \left[C_{L_\alpha}(\beta + i\alpha) + \left(C_{L_q} + C_{L_{\dot{\alpha}}} \right) (\dot{\beta} + i\dot{\alpha}) \frac{d}{V} + \left(C_{y_o} + iC_{L_o} \right) e^{ipt} + C_D(\gamma_y - i\gamma_z) \right] \tag{C1}$$

$$\ddot{y} + i\ddot{z} = -\frac{\rho A}{2m} V^2 [C_L + C_D(\gamma_y - i\gamma_z)] \tag{C1a}$$

where γ_y and γ_z are the projections of the local flight-path angle γ into the y-x and z-x planes, respectively, and z and α data have been corrected for gravity effects. Transforming equation (C1) into x coordinates yields

$$\dot{y} + i\dot{z} = \dot{x}(y' + iz') \tag{C2}$$

$$\ddot{y} + i\ddot{z} = \ddot{x}(y' + iz') + \dot{x} \frac{d(y' + iz')}{dt}$$

$$\ddot{y} + i\ddot{z} = \ddot{x}(y' + iz') + \dot{x}^2(y'' + iz'') \tag{C3}$$

Note that

$$\dot{x} \cong V$$

$$\ddot{x} \cong KV^2[-C_L(\gamma_y - i\gamma_z) - C_D] , \qquad \left(K = \frac{\rho A}{2m} \right)$$

Substituting for $\dot{x}$ and $\ddot{x}$ into equations (C2) and (C3) yields

$$\dot{y} + i\dot{z} = V(y' + iz') \tag{C2a}$$

$$\ddot{y} + i\ddot{z} = KV^2[-C_L(\gamma_y - i\gamma_z) - C_D](y' + iz') + V^2(y'' + iz'') \tag{C3a}$$

If equation (C3a) is substituted into (C1a) with

$$y' + iz' \cong \gamma_y - i\gamma_z$$

the result is

$$y'' + iz'' = -KC_L[1 - (\gamma_y - i\gamma_z)^2]$$

For small γ, as is the case for ballistic range tests, terms of the order γ^2 can be neglected. Then

$$y'' + iz'' = -KC_L$$

$$y'' + iz'' = -K\left[C_{L_\alpha}(\beta + i\alpha) + \left(C_{L_q} + C_{L_{\dot\alpha}}\right)(\beta' + i\alpha')d + \left(C_{y_o} + iC_{L_o}\right)e^{ipx}\right] \tag{C4}$$

After integrating twice with respect to x we obtain

$$y + iz = -K\left[\left(C_{y_o} + iC_{L_o}\right)\left(\frac{1 + ipx - e^{ipx}}{p^2}\right) + C_{L_\alpha}\int_o^x\int_o^x (\beta + i\alpha)dx\,dx\right.$$

$$\left. + (d)\left(C_{L_q} + C_{L_{\dot\alpha}}\right)\int_o^x (\beta + i\alpha)dx - (d)\left(C_{L_q} + C_{L_{\dot\alpha}}\right)(\beta_o + i\alpha_o)x\right]$$

$$+ (y_o' + iz_o')x + (y_o + iz_o) \tag{C5}$$

The integrals are obtained in closed form from the expression for $\beta + i\alpha = K_1e^{\varphi_1 x} + K_2e^{\varphi_2 x} + K_3e^{\varphi_3 x}$. Once the stability routine has been used the only unknowns are C_{y_o}, C_{L_o}, C_{L_α}, $(C_{L_q} + C_{L_{\dot\alpha}})$, y_o', z_o', y_o, and z_o and these appear in a linear fashion and can be found by a straightforward least-squares procedure on the experimental y and z data.

APPENDIX D

ROTATION OF COORDINATES

The purpose of this subroutine is to reduce errors from the small-angle assumption inherent in the tricyclic method by rotating the coordinates so that the maximum resultant angle of attack falls in either the pitch or yaw plane. This is accomplished as follows: After the original gravity-corrected angle data have been curve fit (stability subroutine), that solution is examined to find the maximum resultant angle of attack that occurs nearest the middle of the flight. When it is found, the rotation angle required to bring that resultant angle to the yaw plane is determined.

The experimental θ, ψ, y, and z data are then rotated about the x axis through this angle. If the model is rolling rapidly, the peaks of the motion will be precessing, and this rotation of coordinates may fail to accomplish the stated purpose since successive peaks in the resultant angle of attack will not remain in the β plane.

The angle of rotation, Φ, and the data in the rotated system are printed out for reference. The angle, Φ, is retained so that when all other parts of the data reduction are completed, all information, both data and results, is transformed back to the original reference system.

APPENDIX E

SWERVE CORRECTIONS

The purpose of this subroutine is to correct the flight-path angles α and β to account for swerve of the model. The relations between the earth-fixed angles θ and ψ and the flight-path angles α and β are

$$\alpha = \theta + \tan^{-1} \frac{dz}{dx} \tag{E1}$$

$$\beta = -\psi + \tan^{-1} \frac{dy}{dx} \tag{E2}$$

The procedure for obtaining dz/dx and dy/dx, since they are not known a priori, is as follows: First, since they are small, they are assumed equal to zero initially and the angle data and swerve data are curve fit (stability and lift subroutines). Second, after the initial curve fit to the y and z data (lift routine) is obtained, dz/dx and dy/dx are computed at each data station and new angles α and β are determined. We now recycle through the stability and lift routines to obtain new curve fits. From this new curve fit to the y and z data, new dz/dx and dy/dx are computed. These are compared with the previous set of corrections and if the difference between successive corrections is greater than some input factor, say 0.005°, we again recycle through the stability and lift subroutines. This continues until all corrections are less than 0.005°, at which point the solution is complete.

APPENDIX F

ADDITIONAL FEATURES OF THE PROGRAM

Dividing Tests Into Segments

A provision is available for dividing a given set of flight data into as many segments of any practical length as desired and treating each segment separately. This becomes desirable if the model experiences large velocity losses over the length of the range and if the aerodynamics are sensitive to changes in Mach number or Reynolds number. It may also be desirable for models that have nonlinear aerodynamics with angle of attack and whose maximum amplitudes change significantly over the length of the range. By analyzing segments of such a flight, it is possible to define the variation of aerodynamic coefficients with angle of attack from a single test (provided enough data are collected to define the motion in each segment).

Smoothing Procedure

There is a smoothing procedure that can be used in conjunction with the stability and lift routines. Once the iterative scheme involving stability and lift has converged (that is, when the angle corrections due to swerve are essentially constant), the differences between the experimental and calculated values of α, β, y, and z are examined at each data station. If any are found to be larger than some chosen multiple of the standard deviation of the fit in question, then that experimental value is replaced by the calculated value and the reduction process for stability and lift is repeated. The smoothing process serves two purposes: (1) It tells the experimenter whether some data appear to be in error in comparison to the rest; and (2) by repeating the calculation it shows him what effect this "bad" data had on the derived answers. He can then either check his raw data inputs and resubmit the run or conclude that its effect is small enough to ignore. The number of times the data are smoothed is determined by the user, usually two or three times maximum. If it is done too many times, there is some danger of "walking" the least-squares curves in the direction of the replaced values which could lead to erroneous results.

Partially Missing Data

A provision in the program for weighting the input data (θ, ψ, y, z) from 0 to 1 enables one to place the proper emphasis on each measurement. This is particularly useful if, at some data station, part of the measured data are either poorly defined or missing (for instance, angular measurement is missing in the vertical plane but not in the horizontal). If the data were missing, a weighting factor of 0 would be used (if the data are good, a weighting factor of 1 is automatic). If the data were somewhat uncertain but necessary to obtain results, a weighting factor between 0 and 1, say, 0.5, could be used.

REFERENCES

1. Gray, J. Don; and Lindsay, E. Earl: Force Tests of Standard Hypervelocity Ballistic Models HB-1 and HB-2 at Mach 1.5 to 10. AEDC-TDR-63-137, August 1963.

2. Gray, J. Don: Summary Report on Aerodynamic Characteristics of Standard Models HB-1 and HB-2. AEDC-TDR-64-137, July 1964.

3. Opalka, Klaus O.: Force Tests of the Hypersonic Ballistic Standard Models HB-1 and HB-2. BRL-MR-1798, July 1966.

4. Seiff, Alvin: A New Method for Computing Drag Coefficients from Ballistic Range Data. J. Aero. Sci., vol. 25, no. 2, Feb. 1958, pp. 133-134.

5. Seiff, Alvin; and Wilkins, Max E.: Experimental Investigation of a Hypersonic Glider Configuration at a Mach Number of 6 and at Full-Scale Reynolds Numbers. NASA TN D-341, 1961.

6. Terry, James E.; and Miller, Robert J.: Aerodynamic Characteristics of a Truncated-Cone Lifting Reentry Body at Mach Numbers from 10 to 21. NASA TM X-786, 1963.

7. Nicolaides, John D.: On the Free-Flight Motion of Missiles Having Slight Configurational Asymmetries. BRL Rep. 858, June 1953.

8. Scarborough, J. B.: Numerical Mathematical Analysis. Fourth ed., The Johns Hopkins Press, Baltimore, 1958, pp. 478-484.

9. Allen, H. Julian: Motion of a Ballistic Missile Angularly Misaligned With the Flight Path Upon Entering the Atmosphere and Its Effect Upon Aerodynamic Heating, Aerodynamic Loads, and Miss Distance. NACA TN 4048, 1957.

10. Rasmussen, Maurice L.; and Kirk, Donn B.: On the Pitching and Yawing Motion of a Spinning Symmetric Missile Governed by an Arbitrary Nonlinear Restoring Moment. NASA TN D-2135, 1964.

11. Malcolm, Gerald N.: Stability and Drag Characteristics at Mach Numbers of 10 and 26 of a Proposed Slender Atmospheric Probe. NASA TN D-3917, 1967.

12. Rasmussen, Maurice L.; and Kirk, Donn B.: A Study of Damping in Nonlinear Oscillations. NASA TR R-249, 1966.

13. Chapman, Gary T.; and Kirk, Donn B.: Obtaining Accurate Aerodynamic Force and Moment Results From Ballistic Tests. AGARD Conference Proceedings No. 10, The Fluid Dynamic Aspects of Ballistics, September 5-8, 1966, Mulhouse, France, pp. 381-401. Sponsored by North Atlantic Treaty Organization, Advisory Group for Aerospace Research and Development. Publisher: Harford House, London, 1966.

14. Conn, H.: Ballistic Range Measurement of the Cubic Normal Force and Pitching Moment of a Nonrolling Symmetric Missile. CARDE-TR 569-67, Jan. 1967.

15. Hruby, Ronald J.; McDevitt, John B.; Coon, Grant W.; Harrison, Dean R.; and Kemp, Joseph H., Jr.: FM Telemetry and Free-Flight Techniques for Aerodynamic Measurements in Conventional Wind Tunnels. NASA TN D-3319, 1966.

16. Shinbrot, Marvin: A Least Squares Curve Fitting Method With Applications to the Calculation of Stability Coefficients From Transient-Response Data. NACA TN-2341, 1951.

TABLE I.- TEST DATA

Test	M	$R \times 10^{-6}$	V, ft/sec	C_D	C_{L_α}	$C_{m_{\alpha_l}}$	ξ	$C_{m_q} + C_{m_{\dot{\alpha}}}$	$C_{L_q} + C_{L_{\dot{\alpha}}}$	p, deg/ft	α_m	α_{min}	α_{rms}
(a) Solid models													
[d ≅ 1.25 in., m ≅ 0.0229 slug, x_{cg} ≅ 1.95 d, $I_y \cong 6.2 \times 10^{-4}$ slug-ft^2, $I_x \cong 3.5 \times 10^{-5}$ slug-ft^2]													
1155-1	1.93	1.67	2177	1.308	3.49	-1.490	-16.6	-35.8	16.4	-0.29	6.97	0.69	5.17
1155-2	1.87	1.62	2108	1.321	3.38	-1.429	-18.2	-39.8	14.7	-.29	5.72	.53	4.12
1156	1.96	1.71	2214	1.239	3.59	-1.259	-19.1	-41.5	12.2	-.35	1.80	.17	1.28
1159-1	2.02	1.80	2249	1.249	3.36	-1.490	-15.8	-34.0	18.5	-.30	4.79	.11	3.55
1159-2	1.95	1.74	2172	1.257	3.35	-1.426	-18.6	-40.9	33.1	-.30	3.86	.09	2.74
1160-1	1.99	1.77	2234	1.279	3.31	-1.495	-17.5	-38.3	14.1	-.24	6.84	.41	5.00
1160-2	1.93	1.71	2161	1.284	3.31	-1.416	-19.6	-43.6	25.8	-.24	5.57	.32	3.88
(b) Hollow models													
[d ≅ 1.25 in., m ≅ 0.0141 slug, x_{cg} ≅ 1.95 d, $I_y \cong 2.3 \times 10^{-4}$ slug-ft^2, $I_x \cong 2.1 \times 10^{-5}$ slug-ft^2]													
1197	2.06	1.77	2326	1.236	3.29	-1.517	-23.6	-32.6	6.8	-0.09	7.44	0.60	5.27
1199-1	1.86	1.36	2084	1.249	2.96	-1.128	-21.4	-29.7	6.5	-.14	2.40	.08	1.80
1199-2	1.80	1.31	2014	1.269	2.86	-1.151	-30.8	-44.3	20.7	-.14	1.84	.10	1.19
1199-3	1.73	1.26	1939	1.292	3.04	-1.172	-18.2	-24.9	19.6	-.14	1.08	.23	.95
1200-1	1.99	1.71	2254	1.228	3.33	-1.220	-22.5	-31.1	5.8	-.16	5.44	.46	3.85
1200-2	1.92	1.65	2169	1.246	3.36	-1.140	-23.5	-32.5	23.9	-.16	3.89	.33	2.85
1200-3	1.82	1.56	2056	1.260	3.32	-1.028	-31.2	-44.2	61.8	-.17	2.53	.27	1.66
1203-1	2.07	1.86	2300	1.181	3.21	-1.307	-27.7	-38.5	29.5	-.20	3.89	.30	2.48
1203-2	2.01	1.81	2242	1.192	3.33	-1.288	-31.3	-43.9	28.2	-.20	3.16	.37	2.15
1203-3	1.93	1.74	2150	1.215	3.47	-1.223	-26.6	-36.6	17.8	-.20	1.76	.50	1.26
1203-4	1.86	1.67	2068	1.234	3.02	-1.247	-30.0	-42.4	17.0	-.20	1.20	.39	.85
1204-1	2.08	1.86	2330	1.161	3.29	-1.374	-22.8	-31.5	13.4	-.01	3.10	.44	2.18
1204-2	2.03	1.80	2265	1.179	3.44	-1.296	-24.4	-33.7	15.3	-.01	2.39	.38	1.69
1204-3	1.95	1.74	2181	1.201	3.44	-1.244	-24.4	-33.9	52.7	-.01	1.62	.35	1.25
1204-4	1.87	1.67	2092	1.225	4.02	-1.125	-35.9	-50.5	123.2	-.01	1.12	.48	.81

NATIONAL AERONAUTICS AND SPACE ADMINISTRATION
WASHINGTON, D.C. 20546

OFFICIAL BUSINESS

FIRST CLASS MAIL

POSTAGE AND FEES PAID
NATIONAL AERONAUTICS AND
SPACE ADMINISTRATION

"The aeronautical and space activities of the United States shall be conducted so as to contribute . . . to the expansion of human knowledge of phenomena in the atmosphere and space. The Administration shall provide for the widest practicable and appropriate dissemination of information concerning its activities and the results thereof."

—NATIONAL AERONAUTICS AND SPACE ACT OF 1958

NASA SCIENTIFIC AND TECHNICAL PUBLICATIONS

TECHNICAL REPORTS: Scientific and technical information considered important, complete, and a lasting contribution to existing knowledge.

TECHNICAL NOTES: Information less broad in scope but nevertheless of importance as a contribution to existing knowledge.

TECHNICAL MEMORANDUMS: Information receiving limited distribution because of preliminary data, security classification, or other reasons.

CONTRACTOR REPORTS: Scientific and technical information generated under a NASA contract or grant and considered an important contribution to existing knowledge.

TECHNICAL TRANSLATIONS: Information published in a foreign language considered to merit NASA distribution in English.

SPECIAL PUBLICATIONS: Information derived from or of value to NASA activities. Publications include conference proceedings, monographs, data compilations, handbooks, sourcebooks, and special bibliographies.

TECHNOLOGY UTILIZATION PUBLICATIONS: Information on technology used by NASA that may be of particular interest in commercial and other non-aerospace applications. Publications include Tech Briefs, Technology Utilization Reports and Notes, and Technology Surveys.

Details on the availability of these publications may be obtained from:

SCIENTIFIC AND TECHNICAL INFORMATION DIVISION

NATIONAL AERONAUTICS AND SPACE ADMINISTRATION

Washington, D.C. 20546